Title: Heritable differences in synaptic zinc-transporter levels drive variation in learned birdsong

Authors:

David G. Mets,[1] W. Hamish Mehaffey,[1] Bradley M. Colquitt,[1] and Michael S. Brainard[1,2]

Affiliations

[1] Center for Integrative Neuroscience, University of California, San Francisco, CA 94158; Howard Hughes Medical Institute, University of California, San Francisco, CA 94158.

[2] Departments of Physiology and Psychiatry, University of California, San Francisco, CA 94158.

Abstract:

Complex learned behaviors exhibit striking variation within populations, yet how heritable factors contribute to such inter-individual differences remains largely unknown. Here, we used behavioral-genetic analysis within a Bengalese finch population (*Lonchura striata domestica*) to investigate molecular and circuit mechanisms underlying heritable differences in the tempo of learned birdsong. We identified a genomic locus encoding the zinc transporter ZIP11 and found that *zip11*(*SLC39A11*) transcript was expressed at higher levels in song control circuitry of faster singing birds. Reducing soluble zinc increased synaptic currents in motor circuitry and accelerated song, whereas reducing ZIP11 slowed song. Our results reveal a novel zinc-dependent mechanism that modulates neural activity to drive differences in behavior and suggest that natural variation in learning may preferentially target modulatory processes rather than core neural machinery.

One sentence summary: Heritable levels of a synaptic zinc transporter drive inter-individual differences in circuit excitability and learned song

Main Text:

Natural variation in complex behaviors within a population forms a crucial substrate for selection and, more broadly, is thought to promote the overall success of a species (*1*). However, while recent studies have identified heritable genetic factors that contribute to inter-individual differences in innate behaviors, especially across species (*2–7*), understanding how such factors drive variation in complex learned behaviors within a population remains poorly understood. This reflects in part the dual challenge of needing to disambiguate which aspects of inter-individual differences in learned phenotypes reflect genetic rather than experiential factors and pinpointing the influence of those factors within the distributed neural circuitry that shapes behavior(*8*). Birdsong—a complex motor skill acquired through cultural transmission and subserved by well-delineated neural circuitry (*9–12*)—offers an attractive model(*13*) for studying heritable sources of variation in learned behavior. In particular, song tempo—a defining characteristic of the male's courtship song and motor skill performance more generally (*14–20*)—is shaped both by experience during learning from a tutor and by heritable factors (*21–28*). Moreover, while the characteristic tempo at which an adult bird sings varies by only a few percent from day to day, the tempos at which different individuals sing can span more than a factor of two (*14*, *16*, *29*). Although the precision and reproducibility of song tempo at the level of individual birds has facilitated identification of the neural circuitry that controls song production and enables learning more broadly (*30–39*), the mechanisms that give rise to inter-individual variation, and any specific genetic constraints that govern them, remain unknown. Here, we use an unbiased behavioral-genetic approach to identify a zinc transporter linked to variation in learned song tempo, and then leverage the detailed understanding of birdsong neurobiology to uncover a novel mechanism whereby inter-individual differences in expression of this transporter drive heritable behavioral variation via zinc-dependent modulation of synaptic currents within song control circuitry.

Genetic linkage for song tempo identifies a ZIP-type zinc transporter

To investigate heritable contributions to inter-individual differences in learned song, we first quantified naturally occurring variation in tempo within a genetically heterogeneous breeding population of Bengalese finches maintained by our laboratory (*29*). We collected DNA and recorded the adult songs produced by each individual, as well as the father's tutor song from which they had learned (Fig. 1A). Across the study population, individuals produced songs at tempos (quantified as the median number of syllables sung per second, see Methods) that were strongly correlated with the tempos of their fathers' songs (Fig. 1B, slope = 0.43, r = 0.39, P < 0.0001, two tailed *t*-test). However, even within families in which brothers were tutored by the same father, there could be significant variation in tempo (Fig. 1A-C); some families had narrow, approximately Gaussian distributions of tempo, but many had broad or multi-modal distributions (Fig. 1C). Such non-Gaussian patterns within families suggest the influence of a small number of segregating genetic alleles that have a large impact on song tempo (*40*, *41*), that might therefore be identified through genetic analysis even within modestly sized populations.

To identify genomic regions associated with heritable differences in song tempo, we examined the relationship across the population between inter-individual variation in DNA and song tempo. We first assembled a chromosome-level genome sequence for the Bengalese finch that served as a reference for the analysis (RefSeq assembly accession number GCF_005870125.1, see (*42*) and Methods). For each of 509 birds, from families for which we collected DNA from male offspring and one or both parents, we then sequenced ~400,000 short stretches of DNA (50-65 base pairs) at defined locations distributed throughout the genome (see Methods). We selected approximately 51,000 of these locations that exhibited DNA variation across individuals in the form of single nucleotide polymorphisms (SNPs) and could therefore be used as potentially informative markers for which specific alleles were transmitted from parents to offspring. To assess the strength of association between allelic variation at each locus and variation in tempo, we applied a Transmission Disequilibrium Test (TDT, see Methods and (*43*)). This method takes advantage of knowledge about parentage to restrict analysis for each family to loci that are variable within that family and is comparatively robust to issues arising from population stratification that can confound genome-wide

association studies (*43*, *44*). However, as only a subset of families contributes to allelic variation at a given locus, TDT statistics from adjacent loci within a region are non-redundant and were therefore combined in a sliding window used to scan the genome for regions of interest. To assess statistical significance, we compared the strength of empirically observed associations between genetic variation and tempo against a null distribution of genome-wide maximum values derived from repeating the entirety of the analysis for 10,000 null data sets that preserved the allelic state and familial associations for each bird, but randomly shuffled song tempo (Fig. 1D, S1).

Significant association of allelic state with song tempo was evident for genomic regions on three chromosomes (Fig. 1D, Chromosomes 1, 18, and Z). Moreover, for each of these regions, differences in specific SNPs could account for ~10% differences in tempo across individuals (Fig. 1E, S2). Two of these regions, on Chromosomes 1 and Z, were each relatively large (on the order of megabases) and contained many genes (Fig. S2). However, the region on Chromosome 18 spanned only ~350 kilobases (Fig. 1E), suggesting that substantial variation in tempo might arise from polymorphisms within a single gene. Indeed, a closer examination of this region revealed that the specific allelic variants at five adjacent loci (Fig. 1E) accounted for substantial variation in mean song tempo; for example, at nucleotide 11605768 on Chromosome 18, birds that were homozygous for thymine ('T/T') had an average tempo that was 10.1% faster than for birds that were homozygous for cytosine ('C/C') (Fig. 1F, 7.45 ± 0.06 syl/s vs. 8.20 ± 0.13 syl/s, $P < 0.001$, two tailed *t*-test). These five markers all fall within introns of the avian homolog of the *SLC39A11* (*zip11*) gene, suggesting that variation within this gene or nearby regulatory regions might account for a component of inter-individual variation in learned song tempo.

The predicted avian protein encoded by the *zip11* gene displays 75% identity to the human zinc/iron-regulated transporter-related protein 11 (ZIP 11)—a zinc transporter conserved from yeast to humans and implicated in the import of extracellular zinc to the cytoplasm (*45*). While ZIP11 has primarily been studied in the gut of mammalian systems

(*46*), ZIP-type zinc transporters, including ZIP11, are expressed in the brain (*45*, *47*), where the concentration and distribution of soluble zinc could contribute to neural circuit function (*48*). These observations thus link polymorphisms in a region that encodes the Bengalese finch homolog of the ZIP11 zinc transporter to variation in song tempo, raising the possibility that inter-individual differences in tempo stem in part from heritable differences in zinc regulation.

zip11 is expressed in song premotor circuitry at levels that correlate with song tempo

Previous investigations indicate that song tempo reflects the rate of neural activity propagation within song premotor circuitry, including the telencephalic nucleus HVC (*12*, *30*–*32*, *35*–*39*). Hence, the expression of *zip11* in this circuitry would be well-positioned to influence circuit dynamics underlying song tempo. To evaluate the pattern of *zip11* expression in the avian forebrain, we performed *in situ* hybridization in sagittal brain sections containing HVC. The *zip11* probe labeled cells in both HVC and surrounding tissue (Fig. 2B; boundary of HVC indicated by dashed line). Moreover, most *zip11* labeled cells (83%) were co-labeled with a probe for the excitatory neuronal marker *vglut2* (*SLC17A6*), while most *vglut2* labeled cells (85%) were co-labeled with *zip11*, and the strength of fluorescence signals for these two probes was strongly correlated (Pearson's r of 0.77). Such co-extensive labeling indicates that *zip11* is widely expressed in excitatory neurons both within and around HVC, and raises the possibility that inter-individual differences in the levels of ZIP11 expression within song premotor circuitry contribute to heritable differences in learned song.

To determine whether levels of *zip11* expression differ across birds, and whether any differences correlate with variation in song tempo, we collected mRNA samples from the brains of 17 Bengalese finches that sang at a broad range of tempos. We separately analyzed tissue from HVC and from 'non-song' regions surrounding HVC that contained none of the specialized brain nuclei that have been implicated in song production (Fig. 2C). For each sample, we measured the levels of *zip11* transcript by quantitative polymerase chain reaction. Across individuals, *zip11* transcript levels varied by more than two-fold both in HVC

and in non-song regions; moreover, across individuals, transcript levels in both regions were positively correlated with song tempo, with ~10% change in tempo per fold change in *zip11* (Fig. 2D-E, HVC: r = 0.56, slope = 0.73, P<0.02, two tailed *t*-test; surround: r = 0.65, slope = 0.85, P<0.005, two tailed *t*-test; n = 17 birds from 6 nests). These correlations for non-song regions raise the possibility that ZIP11 may contribute to variation in behaviors other than song, while the correlations within HVC indicate that heritable differences in levels of ZIP11 within song control circuitry could play a causal role in determining inter-individual differences in song tempo.

We next investigated potential mechanisms whereby ZIP11 mediated zinc transport could influence neural circuitry that underlies song tempo. A role for zinc regulation has not figured prominently in models of neural circuit function. However, it has long been appreciated that soluble zinc is present at high levels in the brain, including avian song control regions, and is co-released with glutamate at many central synapses (*49–51*). Moreover, zinc exerts widespread modulatory effects on both voltage and ligand-gated ion channels, and several recent studies indicate that zinc manipulations can alter synaptic and circuit function (*52–57*). To investigate how ZIP11 might influence neural activity in HVC, we assessed the subcellular localization of ZIP11 protein using a commercially available antibody raised against a portion of mouse ZIP11 that is 99% homologous to the same region of Bengalese finch ZIP11 (see Methods). Immunofluorescent labeling revealed that ZIP11 protein is enriched in discrete puncta that almost completely co-localize with an antibody directed to VGLUT2, which specifically marks glutamatergic synapses (Fig. 3B, MERGE, Pearson's r of 0.72 between ZIP11 and VGLUT2 antibody staining; 68% of ZIP11 puncta were positive for VGLUT2 protein and 70% of VGLUT2 puncta were positive for ZIP11 protein). This distribution of the ZIP11 transporter suggests that it could modulate activity within the HVC microcircuit by shaping the level and distribution of soluble zinc at excitatory synapses.

We explored the potential role of zinc in modulating synaptic transmission within HVC by assessing the effects of zinc chelation on evoked currents in a brain slice preparation. We elicited antidromic action potentials in premotor HVC neurons that project to RA (HVC-RA neurons) by stimulating the fiber tract leading to RA, outside of the boundaries of HVC (Fig.

3C). The axons of HVC-RA neurons make extensive local synapses within HVC (*58–60*). Hence, by antidromically activating HVC-RA neurons and measuring excitatory post-synaptic currents (EPSCs) in other downstream HVC neurons, we could assay the effects of zinc manipulation on circuit components that contribute to the propagation of neural activity within HVC and the control of song timing. We used intracellular recordings to first identify an individual HVC neuron in which EPSCs could be driven by antidromic stimulation, and then measured changes to EPSCs following bath application of a zinc chelator [TPEN [N,N,N,N-tetrakis (2-pyridinylmethyl)-1,2-ethanediamine] or ZX1 (see Methods)]. Consistent with reports in other systems (*53*, *56*), we found that zinc chelation in HVC increased post-synaptic drive. In some cases, there was a simple scaling in the magnitude of the EPSC elicited by antidromic stimulation (Figs. 3D and S3A). In other cases, there was also an increase in polysynaptic events after stimulation (Fig. S3B). Correspondingly, we found that zinc chelation caused an increase in both the peak amplitude of EPSCs (Fig. 3E, 18 ± 5% increase after chelation, P <0.005, paired t-test, n = 12 experiments, n = 6 birds) and the total charge transfer (Fig. S3C, 26.5 ± 10% increase after chelation, P <0.01, paired t-test, n = 12 experiments, n = 6 birds). These electrophysiological measurements indicate that reducing soluble zinc increases the amplitude of EPSCs within HVC and the overall excitability of the HVC microcircuit. Such marked *in vitro* effects of zinc manipulation on the excitability within the HVC circuit suggest that regulation of Zn^{2+} levels, including through ZIP11, has the potential to influence the speed of activity propagation through HVC, and prompted us to next evaluate if perturbing this system *in vivo* in adult birds would directly alter the tempo of learned song.

Levels of soluble zinc and Zip11 are causally linked to song tempo

We tested whether zinc levels can influence the tempo of adult song by measuring changes to song following systemic injections of the zinc chelator, clioquinol (CQ), an established, non-toxic means of reducing levels of soluble zinc in behaving animals (*61*). CQ injection markedly increased song tempo across all experiments (Fig. 4A-D, top, 6.2 ± 1.7% average increase in median tempo for n = 6 birds, range 0.3 – 0.9 syl/s, P < 0.02 for each bird, Mood's median test). In contrast, tempo was unaffected following injection of vehicle

alone (Fig. 4A-D, bottom; 0.59 ± 0.25% average change in median tempo for n = 6 birds, P > 0.1 for each bird, Mood's median test). Notably, neither CQ (Fig. 4A, 'Experimental') nor vehicle (Fig. 4A, 'Control') caused apparent changes to the number or spectral structure of song syllables (Fig. 4B, compare 'Pre' to 'Post').

To more directly link ZIP11 levels to song tempo, we evaluated the effect of reducing ZIP11 selectively in HVC by using small interfering RNAs (siRNAs, (*62*)). We designed several siRNAs to target *zip11* transcript and screened these in Bengalese finch primary neural cultures to identify candidates causing ~50% reduction of endogenous *zip11* transcript (Fig. S2). We then injected anti-*zip11* siRNA complexed with a transfection agent bilaterally into HVC of adult birds and measured the impact on learned song tempo (Fig. 4E-H, Experimental). For each individual injected with anti-*zip11* siRNA, a co-reared brother was injected with a control siRNA that targeted no known Bengalese finch transcript (Fig. 4E-H, Control). Neither injection caused immediate changes to song structure. However, 48 hours after the injection, the songs of all birds in the 'Experimental' group were significantly slowed relative to their pre-injection values (Fig. 4F-H, top, -7.0 ± 1.8% average change in median tempo, n = 4 birds; P < 0.02 for each bird, Mood's median test). In contrast, the control group displayed no changes to song tempo (Fig. 4F-H, bottom, 0.90 ± 0.5% average change in median tempo), n = 4 brothers; P > 0.1 for each bird). The consistent effects of reducing *zip11* transcript on song tempo demonstrate that differences in ZIP11 levels within HVC can account causally for inter-individual differences in this complex learned phenotype.

Discussion:

It is widely appreciated that behavior is shaped by an interplay of genetics and experience (*8*). However, the mechanisms whereby heritable factors contribute to inter-individual differences in learned behaviors are still poorly understood. Our findings demonstrate the efficacy of an unbiased behavioral-genetic approach in proceeding from a phenotype of interest to underlying mechanisms that contribute to inter-individual variation. In the songbird, this approach enabled the identification of three genomic regions that each

account for ~10% variation in the tempo of learned song, and revealed a novel zinc-dependent mechanism that modulates circuit function and behavior. These findings begin to bridge the gap between the genetic, circuit, and behavioral levels of inter-individual variation in learned behaviors and raise the possibility that one way by which evolution has achieved a balance between individuality and robustness is by targeting modulatory processes rather than the core machinery of circuit function.

Our unbiased behavioral-genetic approach to identifying specific sources of inter-individual variation in song complements studies that seek a general understanding of circuit function through neural recordings and circuit perturbations. For birdsong, such prior work has provided a detailed account of song control circuitry and linked the rate of neural activity propagation in HVC to the precise timing of song (*12*, *30–32*, *34–38*). However, despite this understanding, even extensive measurements of how song circuitry differs across individuals could, at best, identify only correlative evidence regarding what causes some birds to sing at over twice the tempo of others (*14*, *28*, *29*, *63*). Here, a behavioral-genetic approach enabled us to proceed in a directed fashion from inter-individual variation in tempo towards underlying causal mechanisms mediated by differences in ZIP11 levels at glutamatergic synapses in HVC. While we focused in this study on *zip11*, we also identified two other regions of the genome where inter-individual differences had large effects on tempo (~10%). The ability to detect genomic regions that have such large effects on behavior likely derives from the structure of our study, which examines how the transmission of alleles within each family contributes to phenotypic variation; this approach is similar to hybridization studies or rare variant studies in human pedigrees, in which a limited number of genetic variants within a population may contribute to large inter-individual differences in phenotypes. In this respect, we expect that examination of different Bengalese finch pedigrees, or genome-wide associational studies across larger populations, would reveal additional genomic regions linked to tempo. More broadly, our results support the potential of such approaches in systems such as the songbird—where behavior is subserved by well-delineated neural circuity—in identifying and pinpointing novel mechanisms that drive inter-individual variation in complex phenotypes.

Although zinc modulation does not play a prominent role in most contemporary models of circuit dynamics, our findings support the idea that active regulation of zinc levels may constitute a general mechanism for modulating behaviorally relevant neural activity. Indeed, not only is zinc co-released with glutamate at many central synapses, but work in mammalian systems indicates that artificial manipulation of soluble zinc by chelation can alter synaptic and circuit function both *in vitro* and *in vivo (49, 53, 55, 56, 64)*. While zinc interacts with a multitude of biological processes that are potentially relevant to circuit function (*48*, *51*, *52*), it is noteworthy in the context of our results that synaptic zinc, co-released with glutamate, can act directly on glutamate receptors to attenuate excitatory post-synaptic currents (*53*, *56*). Hence, zinc chelation may increase synaptic currents in HVC and speed song by reducing levels of synaptic zinc, while higher levels of ZIP11—which is a member of a class of transporters that import zinc from extracellular space to the cytoplasm (*45*, *47*, *65*)—may similarly contribute to faster songs by reducing levels of soluble zinc at the synapse. Moreover, our finding that *zip11* levels are correlated between song and non-song regions raises the possibility that heritable differences in ZIP11 may influence the excitability and temporal dynamics of neural circuits underlying a variety of other behaviors in a coordinated fashion. Indeed, given the widespread expression of ZIP transporters, including ZIP11, in the nervous systems of species ranging from nematodes to humans, our results suggest that similar zinc-dependent processes may be an evolutionarily conserved mechanism for modulating multiple aspects of neural circuit function and behavior (*47*, *66*).

The mechanisms that we have identified in adult birds may also play a role in the earliest stages of song learning, as HVC is implicated not only in song production but also in the sensory learning of the tutor song in juvenile birds (*67*, *68*). It has long been hypothesized that such learning is constrained by an innate “template” that establishes a bias for birds to learn preferentially from songs of their own species (*21*, *25*, *27*, *69–72*), and our prior work has extended this idea by showing that individual birds within a species learn most effectively when they are presented with tutor songs at tempos that match their individual innate predispositions (*28*). However, while the concept of templates that constrain which stimuli are

effective in guiding learning has been highly influential, how such biases are instantiated at a circuit level remains unclear. Our results suggest that such biases could result in part from a concordance between the structure of instructive sensory stimuli and the biophysically determined properties of the circuits upon which they act(*73*). For example, if ZIP11 contributes to differences in the temporal dynamics of HVC circuitry(*16*, *36*, *38*, *74*) even prior to tutoring, then tutor songs at the appropriately matched tempo may more effectively drive the cellular and circuit changes that instantiate sensory learning. More broadly, this suggests that innate differences in circuit biophysics may lead to a distribution, within the population, of sensitivities to specific statistics of the natural world that enable some individuals to learn better from, and perhaps seek, experiences that match their predispositions (*22*, *23*, *26*, *28*, *71*, *75*, *76*).

The correlation between *zip11* expression and song tempo even in non-song brain regions indicates that ZIP11 may contribute to variation in diverse other behaviors subserved by those regions. Most simply, this might include variation in the temporal dynamics of other movements; however, it likewise could include variation along any axis of behavior that is influenced by changes to the synaptic strength or excitability within underlying neural circuitry. This is especially interesting from the perspective that song is a courtship behavior that female birds use in part to select their mates (*17*, *20*). The joint influences of experience and heritability on tempo render it an informative signal about the relatedness of the singer (*77*, *78*), while the possibility that other behavioral traits covary with tempo suggests that It might additionally provide females with signals about inter-individual differences that are relevant to assessment of a male's fitness and compatibility. These considerations raise intriguing questions for future work regarding what constellation of behavioral traits covary with heritable differences in song structure and whether females are attentive to the aspects of song structure that encode such behavioral variation.

Finally, we note that the relative obscurity, from the standpoint of contemporary circuit models, of ZIP-dependent changes in circuit dynamics may reflect a more general principle regarding the generation of natural variation in behavior. In particular, while inter-individual

variation in behavior is an evolutionary imperative, it cannot arise at the expense of fundamental circuit functionality. Thus, while circuit perturbations or mutagenesis that grossly disrupt behaviors can reveal critical components of neural machinery, our findings suggest that investigations of naturally occurring variation may preferentially uncover more subtle mechanisms—such as the modulatory processes described here—that enable inter-individual differences within a population while leaving intact the indispensable parts of brain function.

References and Notes

1. A. Forsman, L. Wennersten, Inter-individual variation promotes ecological success of populations and species: evidence from experimental and comparative studies. *Ecography.* **39**, 630–648 (2016).

2. P. T. McGrath *et al.*, Parallel evolution of domesticated Caenorhabditis species targets pheromone receptor genes. *Nature*. **477**, 321–325 (2011).

3. A. K. Greenwood, A. R. Wark, K. Yoshida, C. L. Peichel, Genetic and neural modularity underlie the evolution of schooling behavior in threespine sticklebacks. *Curr. Biol.* **23**, 1884–1888 (2013).

4. J. Shorter *et al.*, Genetic architecture of natural variation in Drosophila melanogaster aggressive behavior. *Proc. Natl. Acad. Sci. U. S. A.* **112**, E3555–E3563 (2015).

5. Y. Ding, A. Berrocal, T. Morita, K. D. Longden, D. L. Stern, Natural courtship song variation caused by an intronic retroelement in an ion channel gene. *Nature*. **536**, 329–332 (2016).

6. A. Bendesky *et al.*, The genetic basis of parental care evolution in monogamous mice. *Nature*. **544**, 434–439 (2017).

7. N. Niepoth, A. Bendesky, How Natural Genetic Variation Shapes Behavior. *Annu. Rev. Genomics Hum. Genet.* **21**, 437–463 (2020).

8. J. B. S. Haldane, Some Principles of Causal Analysis in Genetics. *Erkenntnis*. **6**, 346–357 (1936).

9. F. Nottebohm, T. M. Stokes, C. M. Leonard, Central control of song in the canary, Serinus canarius. *J. Comp. Neurol.* **165**, 457–486 (1976).

10. P. J. B. Slater, The cultural transmission of bird song. *Trends Ecol. Evol.* **1**, 94–97 (1986).

11. A. J. Doupe, P. K. Kuhl, Birdsong and human speech: common themes and mechanisms. *Annu. Rev. Neurosci.* **22**, 567–631 (1999).

12. A. Nieder, R. Mooney, The neurobiology of innate, volitional and learned vocalizations in mammals and birds. *Philos. Trans. R. Soc. B Biol. Sci.* **375** (2020), doi:10.1098/rstb.2019.0054.

13. G. Laurent, On the value of model diversity in neuroscience. *Nat. Rev. Neurosci.*, doi:10.1038/s41583-020-0323-1.

14. J. Podos, A Performance Constraint on the Evolution of Trilled Vocalizations in a Songbird Family (Passeriformes: Emberizidae). *Evolution.* **51**, 537 (1997).

15. M. D. Mauk, D. V. Buonomano, The Neural Basis of Temporal Processing. *Annu. Rev. Neurosci.* **27**, 307–340 (2004).

16. J. F. Prather, S. Nowicki, R. C. Anderson, S. Peters, R. Mooney, Neural correlates of categorical perception in learned vocal communication. *Nat. Neurosci.* **12**, 221–228 (2009).

17. J. Byers, E. Hebets, J. Podos, Female mate choice based upon male motor performance. *Anim. Behav.* **79**, 771–778 (2010).

18. D. C. Lahti, D. L. Moseley, J. Podos, A Tradeoff Between Performance and Accuracy in Bird Song Learning. *Ethology*. **117**, 802–811 (2011).

19. D. Deutsch, J. Clemens, S. Y. Thiberge, G. Guan, M. Murthy, Shared Song Detector Neurons in Drosophila Male and Female Brains Drive Sex-Specific Behaviors. *Curr. Biol.* **29**, 3200-3215.e5 (2019).

20. J. L. Dunning, S. Pant, K. Murphy, J. F. Prather, Female finches prefer courtship signals indicating male vigor and neuromuscular ability. *PLoS One*. **15**, e0226580 (2020).

21. M. Konishi, The Role of Auditory Feedback in the Control of Vocalization in the White-Crowned Sparrow1. *Z. Tierpsychol.* **22**, 770–783 (1965).

22. P. Marler, S. Peters, Selective vocal learning in a sparrow. *Science*. **198**, 519–21 (1977).

23. P. C. Mundinger, Behaviour-genetic analysis of canary song: inter-strain differences in sensory learning, and epigenetic rules. *Anim. Behav.* **50**, 1491–1511 (1995).

24. J. Podos, S. Nowicki, S. Peters, Permissiveness in the learning and development of song syntax in swamp sparrows. *Anim. Behav.* **58**, 93–103 (1999).

25. T. J. Gardner, F. Naef, F. Nottebohm, Freedom and rules: the acquisition and reprogramming of a bird's learned song. *Science*. **308**, 1046–9 (2005).

26. O. Fehér, H. Wang, S. Saar, P. P. Mitra, O. Tchernichovski, De novo establishment of wild-type song culture in the zebra finch. *Nature*. **459**, 564–568 (2009).

27. A. L. Lansverk *et al.*, The variability of song variability in zebra finch (*Taeniopygia guttata*) populations. *R. Soc. Open Sci.* **6**, 190273 (2019).

28. D. G. Mets, M. S. Brainard, Learning is enhanced by tailoring instruction to individual genetic differences. *eLife*. **8** (2019), doi:10.7554/eLife.47216.

29. D. G. Mets, M. S. Brainard, Genetic variation interacts with experience to determine interindividual differences in learned song. *Proc. Natl. Acad. Sci. U. S. A.* **115**, 421–426 (2018).

30. Z. Chi, D. Margoliash, Temporal precision and temporal drift in brain and behavior of zebra finch song. *Neuron*. **32**, 899–910 (2001).

31. R. H. R. Hahnloser, A. A. Kozhevnikov, M. S. Fee, An ultra-sparse code underlies the generation of neural sequences in a songbird. *Nature*. **419**, 65–70 (2002).

32. M. A. Long, M. S. Fee, Using temperature to analyse temporal dynamics in the songbird motor pathway. *Nature*. **456**, 189–194 (2008).

33. J. H. Goldberg, M. S. Fee, A cortical motor nucleus drives the basal ganglia-recipient thalamus in singing birds. *Nat. Neurosci.* **15**, 620–627 (2012).

34. M. S. Brainard, A. J. Doupe, Translating birdsong: songbirds as a model for basic and applied medical research. *Annu. Rev. Neurosci.* **36**, 489–517 (2013).

35. M. F. Schmidt, J. Martin Wild, The respiratory-vocal system of songbirds: anatomy, physiology, and neural control. *Prog. Brain Res.* **212**, 297–335 (2014).

36. J. E. Markowitz *et al.*, Mesoscopic patterns of neural activity support songbird cortical sequences. *PLoS Biol*. **13**, 1–20 (2015).

37. K. Hamaguchi, M. Tanaka, R. Mooney, A Distributed Recurrent Network Contributes to Temporally Precise Vocalizations. *Neuron*. **91**, 680–693 (2016).

38. Y. S. Zhang, J. D. Wittenbach, D. Z. Jin, A. A. Kozhevnikov, Temperature manipulation in songbird brain implicates the premotor nucleus HVC in birdsong syntax. *J. Neurosci.* **37**, 2600–2611 (2017).

39. R. Egger *et al.*, Local Axonal Conduction Shapes the Spatiotemporal Properties of Neural Sequences. *Cell*. **183**, 537–548.e12 (2020).

40. K. Hammond, J. W. James-R, Genes of Large Effect and the Shape of the Distribution of a Quantitative Character. *Aus. J. Biol. Sci.* **4**, 867–876 (1970).

41. M. Lynch, B. Walsh, *Genetics and analysis of quantitative traits* (Sinauer, 1998).

42. B. M. Colquitt, D. G. Mets, M. S. Brainard, Draft genome assembly of the Bengalese finch, Lonchura striata domestica, a model for motor skill variability and learning. *Gigascience*. **7**, 1–6 (2018).

43. R. S. Spielman, R. E. McGinnis, W. J. Ewens, Transmission test for linkage disequilibrium: The insulin gene region and insulin-dependent diabetes mellitus (IDDM). *Am. J. Hum. Genet.* **52**, 506–516 (1993).

44. M. M. Xiong, J. Krushkal, E. Boerwinkle, TDT statistics for mapping quantitative trait loci. *Ann. Hum. Genet.* **62**, 431–452 (1998).

45. Y. Yu *et al.*, Characterization of the GufA subfamily member SLC39A11/Zip11 as a zinc transporter. *J. Nutr. Biochem.* **24**, 1697–1708 (2013).

46. R. J. Cousins *et al.*, Gastric and colonic zinc transporter ZIP11 (Slc39a11) in mice responds to dietary zinc and exhibits nuclear localization. *J. Nutr.* **143**, 1882–1888 (2013).

47. J. Jeong, D. J. Eide, The SLC39 family of zinc transporters. *Mol. Aspects Med.* **34**, 612–619 (2013).

48. L. J. Blakemore, P. Q. Trombley, Zinc as a neuromodulator in the central nervous system with a focus on the olfactory bulb. *Front. Cell. Neurosci.* **11** (2017), doi:10.3389/fncel.2017.00297.

49. G. A. Howell, M. G. Welch, C. J. Frederickson, Stimulation-induced uptake and release of zinc in hippocampal slices. *Nature*. **308**, 736–738 (1984).

50. C. M. Montagnese, F. A. Geneser, J. R. Krebs, Histochemical distribution of zinc in the brain of the zebra finch (Taenopygia guttata). *Anat. Embryol. (Berl).* **188**, 173–187 (1993).

51. C. E. Brown, R. H. Dyck, Distribution of zincergic neurons in the mouse forebrain. *J. Comp. Neurol.* **479**, 156–167 (2004).

52. E. P. Huang, Metal ions and synaptic transmission: Think zinc. *Proc. Natl. Acad. Sci. U. S. A.* **94**, 13386–13387 (1997).

53. K. Vogt, J. Mellor, G. Tong, R. Nicoll, The Actions of Synaptically Released Zinc at Hippocampal Mossy Fiber Synapses. *Neuron*. **26**, 187–196 (2000).

54. A. M. Vergnano *et al.*, Zinc Dynamics and Action at Excitatory Synapses. *Neuron*. **82**, 1101–1114 (2014).

55. C. T. Anderson *et al.*, Modulation of extrasynaptic NMDA receptors by synaptic and tonic zinc. *Proc. Natl. Acad. Sci. U. S. A.* **112**, E2705–E2714 (2015).

56. B. I. Kalappa, C. T. Anderson, J. M. Goldberg, S. J. Lippard, T. Tzounopoulos, AMPA receptor inhibition by synaptically released zinc. *Proc. Natl. Acad. Sci. U. S. A.* **112**, 15749–15754 (2015).

57. A. Joshi *et al.*, Cell-Specific Activity-Dependent Fractionation of Layer 2/3->5B Excitatory Signaling in Mouse Auditory Cortex. *J. Neurosci.* **35**, 3112–3123 (2015).

58. R. Mooney, J. F. Prather, The HVC microcircuit: The synaptic basis for interactions between song motor and vocal plasticity pathways. *J. Neurosci.* **25**, 1952–1964 (2005).

59. G. Kosche, D. Vallentin, M. A. Long, Interplay of inhibition and excitation shapes a premotor neural sequence. *J. Neurosci.* **35**, 1217–1227 (2015).

60. J. Kornfeld *et al.*, EM connectomics reveals axonal target variation in a sequence-generating network. *eLife*. **6** (2017), doi:10.7554/eLife.24364.

61. Y. B. Nitzan *et al.*, Clioquinol effects on tissue chelatable zinc in mice. *J. Mol. Med.* **81**, 637–644 (2003).

62. S. M. Elbashir *et al.*, Duplexes of 21-nucleotide RNAs mediate RNA interference in cultured mammalian cells. *Nature*. **411**, 494–498 (2001).

63. H. Kagawa *et al.*, Ecological correlates of song complexity in white-rumped munias. *Interact. Stud. Soc. Behav. Commun. Biol. Artif. Syst. Stud. / Soc. Behav. Commun. Biol. Artif. Syst. Stud.* **13**, 263–284 (2012).

64. C. T. Anderson, M. Kumar, S. Xiong, T. Tzounopoulos, Cell-specific gain modulation by synaptically released zinc in cortical circuits of audition. *eLife*. **6**, 1–20 (2017).

65. M. Lou Guerinot, The ZIP family of metal transporters. *Biochim. Biophys. Acta - Biomembr.* **1465**, 190–198 (2000).

66. G. Davies *et al.*, Study of 300,486 individuals identifies 148 independent genetic loci influencing general cognitive function. *Nat. Commun.* **9** (2018), doi:10.1038/s41467-018-04362-x.

67. T. F. Roberts, S. M. H. Gobes, M. Murugan, B. P. Ölveczky, R. Mooney, Motor circuits are required to encode a sensory model for imitative learning. *Nat. Neurosci.* **15**, 1454–1459 (2012).

68. W. Zhao, F. Garcia-Oscos, D. Dinh, T. F. Roberts, Inception of memories that guide vocal learning in the songbird. *Science.* **366**, 83–89 (2019).

69. P. Marler, A comparative approach to vocal learning: Song development in white-crowned sparrows. *J. Comp. Physiol. Psychol.* **71**, 1–25 (1970).

70. J. Soha, The auditory template hypothesis: a review and comparative perspective. *Anim. Behav.* **124**, 247–254 (2017).

71. J. A. Soha, P. Marler, A species-specific acoustic cue for selective song learning in the white-crowned sparrow. *Anim. Behav.* **60**, 297–306 (2000).

72. D. A. Nelson, A preference for own-subspecies' song guides vocal learning in a song bird. *Proc. Natl. Acad. Sci. U. S. A.* **97**, 13348–13353 (2000).

73. M. Rabinovich, R. Huerta, G. Laurent, Transient Dynamics for Neural Processing. *New Ser.* **321**, 48–50 (2008).

74. K. E. Bouchard, M. S. Brainard, Auditory-induced neural dynamics in sensory-motor circuitry predict learned temporal and sequential statistics of birdsong. *Proc. Natl. Acad. Sci. U. S. A.* **113**, 9641–9646 (2016).

75. D. A. Nelson, A preference for own-subspecies' song guides vocal learning in a song bird. *Proc. Natl. Acad. Sci. U. S. A.* **97**, 13348–13353 (2000).

76. P. C. Mundinger, D. C. Lahti, Quantitative integration of genetic factors in the learning and production of canary song. *Proc. R. Soc. B Biol. Sci.* **281** (2014), doi:10.1098/rspb.2013.2631.

77. A. F. G. Bourke, Hamilton's rule and the causes of social evolution. *Philos. Trans. R. Soc. B Biol. Sci.* **369** (2014), doi:10.1098/rstb.2013.0362.

78. A. E. Leedale *et al.*, Cost, risk, and avoidance of inbreeding in a cooperatively breeding bird. *Proc. Natl. Acad. Sci. U. S. A.* **117**, 15724–15730 (2020).

79. E. Lieberman-Aiden *et al.*, Comprehensive mapping of long-range interactions reveals folding principles of the human genome. *Science.* **326**, 289–293 (2009).

80. B. K. Peterson, J. N. Weber, E. H. Kay, H. S. Fisher, H. E. Hoekstra, Double Digest RADseq: An Inexpensive Method for De Novo SNP Discovery and Genotyping in Model and Non-Model Species. *PLoS One*. **7**, e37135 (2012).

81. H. Li, Aligning sequence reads, clone sequences and assembly contigs with BWA-MEM (2013) (available at http://arxiv.org/abs/1303.3997).

82. H. Li, R. Durbin, Fast and accurate short read alignment with Burrows-Wheeler transform. *Bioinformatics*. **25**, 1754–1760 (2009).

83. A. McKenna *et al.*, The genome analysis toolkit: A MapReduce framework for analyzing next-generation DNA sequencing data. *Genome Res.* **20**, 1297–1303 (2010).

84. S. Zhang, Q. Sha, H. S. Chen, J. Dong, R. Jiang, Transmission/disequilibrium test based on haplotype sharing for tightly linked markers. *Am. J. Hum. Genet.* **73**, 566–579 (2003).

85. E. M. M. Manders, F. J. Verbeek, J. A. Aten, Measurement of co-localization of objects in dual-colour confocal images. *J. Microsc.* **169**, 375–382 (1993).

86. J. Kosubek-Langer, L. Schulze, C. Scharff, Maturation, behavioral activation, and connectivity of adult-born medium spiny neurons in a striatal song nucleus. *Front. Neurosci.* **11**, 323 (2017).

Acknowledgements:
The authors thank A. Karpova, D. Manoli, E. Merfeld, M. Scanziani, and J. Willsey for discussions and comments on the manuscript.

Funding:
Howard Hughes Medical Institute (MSB)
Program for Breakthrough Biomedical Research award from the Sandler Family Foundation (MSB)
The Jane Coffin Childs Fund for Medical Research (DGM)

Author contributions:
Conceptualization: DGM, MSB
Methodology: DGM, WHM, BMC
Investigation: DGM, WHM, BMC
Writing-original draft: DGM, MSB
Writing-review & editing: DGM,WHM,BMC,MSB

Competing interests:
Authors declare that they have no competing interests.

Data and materials availability:
All data are available in the main text or the supplementary materials.

Supplementary Materials
Materials and Methods
Figs. S1 to S4
Tables S1 to S4
Data S1

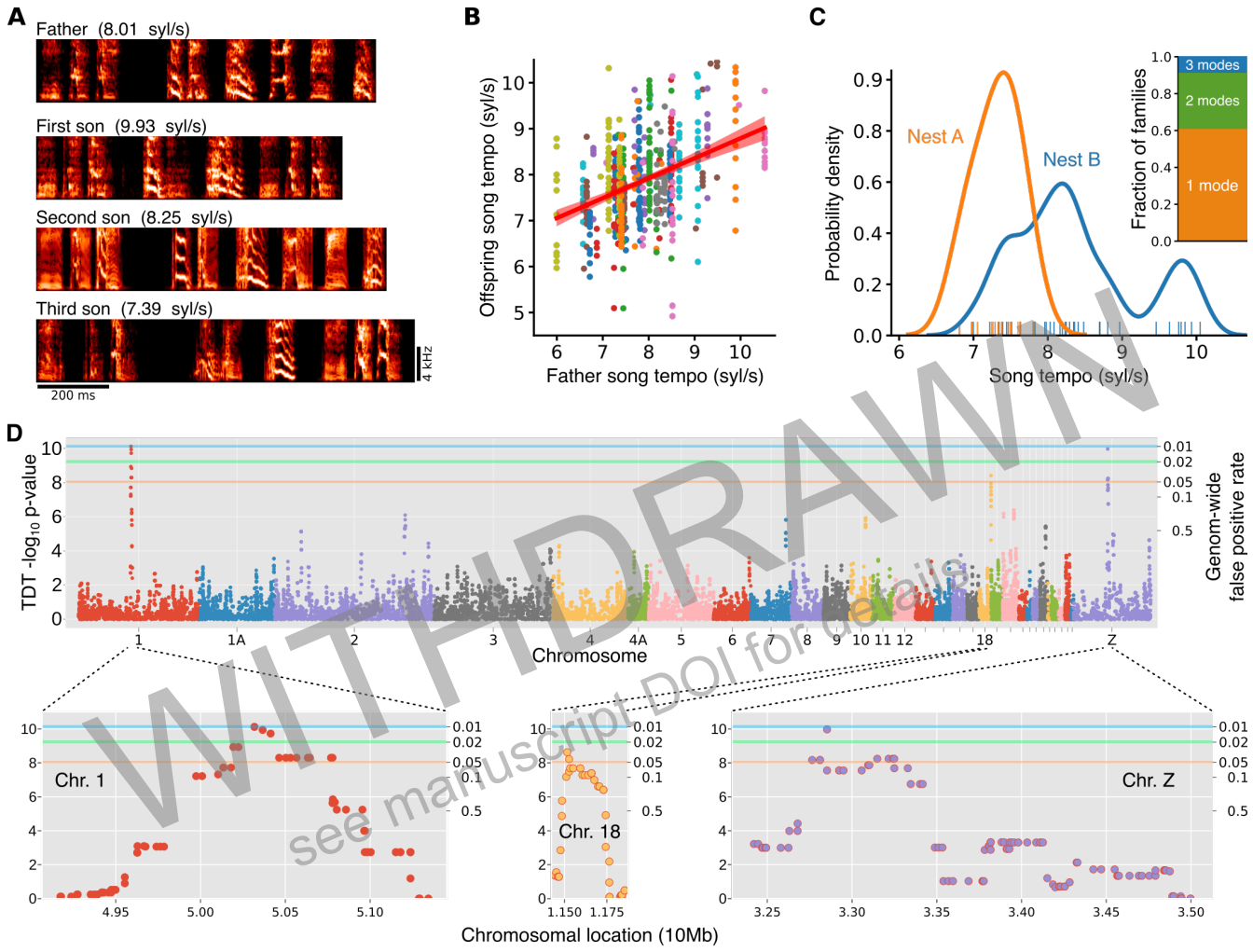

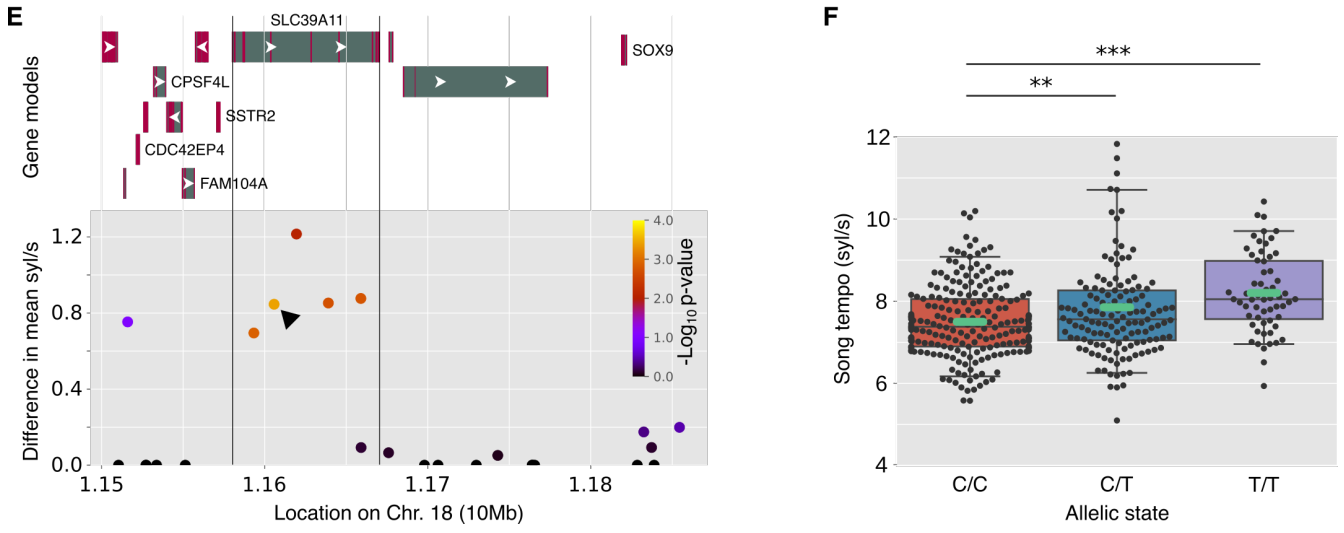

Fig. 1. Genetic mapping identifies genomic regions influencing song tempo.

(A) Example songs from a father (top) and three of his sons (bottom). The sons produced copies of their father's song that were generally similar in multiple features, including the repertoire of discrete syllables, their ordering, and the tempo at which they were produced, but there was also variation in these features across individuals. (B) Relationship between the tempo of the father's song and the tempo of songs produced by his offspring (n = 572 offspring from 54 fathers/nests, r = 0.39, slope = 0.43, P < 0.0001). The significant correlation across families reflects the potential influence of both the father's tutor song, and his transmitted genes. The variation within families (vertically aligned points), despite the same tutor, could reflect individual differences in transmitted genes that affect tempo. (C) Probability distribution of tempo for two families, one with a single mode (orange) and a second with multiple modes (blue). More than one mode was present in ~40% of families and is consistent with segregating genes of large effect (right, number of modes determined by the minimum Bayesian information criterion from Gaussian mixture model fits). (D) Genome wide scan for linkage between molecular-genetic markers and song tempo. Left Y axis indicates the p-value of the TDT test statistic calculated for each sliding window of 20 markers. Right Y axis indicates permutation based genome-wide false positive rate. Expanded views of significant peaks are shown below (n = 509 birds; colored lines indicate permutation based genome-wide significance thresholds of P = 0.05 (orange), P = 0.02 (green), and P = 0.01 (blue)). (E) Difference in mean tempo between allelic states for single markers (SNPs) on the right end of Chromosome 18 plotted against their genomic position. Significance is indicated by marker color. Gene models derived from genome annotation are indicated at top. Arrows indicate coding direction. Introns are shown in green, exons are shown in purple. Black arrow indicates marker shown in F. (F) Distribution of song tempos for birds of each of three allelic states (C/C, C/T, T/T) found at nucleotide 11605768 on Chromosome 18. Birds with T/T sang significantly faster than birds with C/C (two tailed *t*-test; ** P < 0.02; *** P < 0.0001) consistent with linkage between allelic state at this location and tempo. Means indicated by cyan bars. Box shows median and inner quartiles and whiskers show 5th and 95th percentiles.

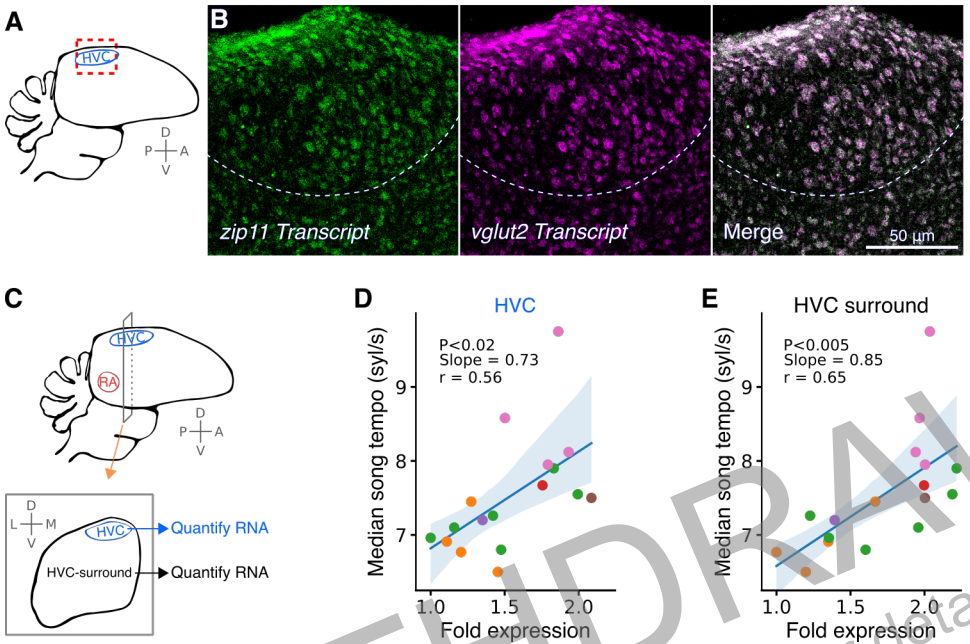

Fig. 2. *zip11* mRNA transcript levels in HVC correlate with song tempo.

A) Sagittal section illustrating the brain area imaged for *zip11* transcript (red). (B) Dual *In situ* mRNA hybridization to *zip11* (*SLC39A11*) transcript (left) and *vglut2* (*SLC17A6*) transcript (middle). The merge (right) reveals co-localization indicating that *zip11* is expressed in excitatory neurons in the avian forebrain. Dashed line indicates the boundary of HVC. (C) Schematic illustrating tissue separation used to assess transcript levels. We dissected coronal sections of forebrain tissue into samples containing the song premotor nucleus HVC (blue) and surrounding non-song brain tissue anterior to the song premotor nucleus RA (black, HVC-surround). *zip11* transcript levels for each region were determined by quantitative polymerase chain reaction. (D, E) Inter-individual differences in *zip11* transcript levels in HVC (D) and HVC-surround (E) were positively correlated with the song tempo of individual birds (n = 17 birds from 6 nests; nests indicated by color). Fold expression changes are relative to the lowest expression level in the set. Parameters were fit by ordinary least squares.

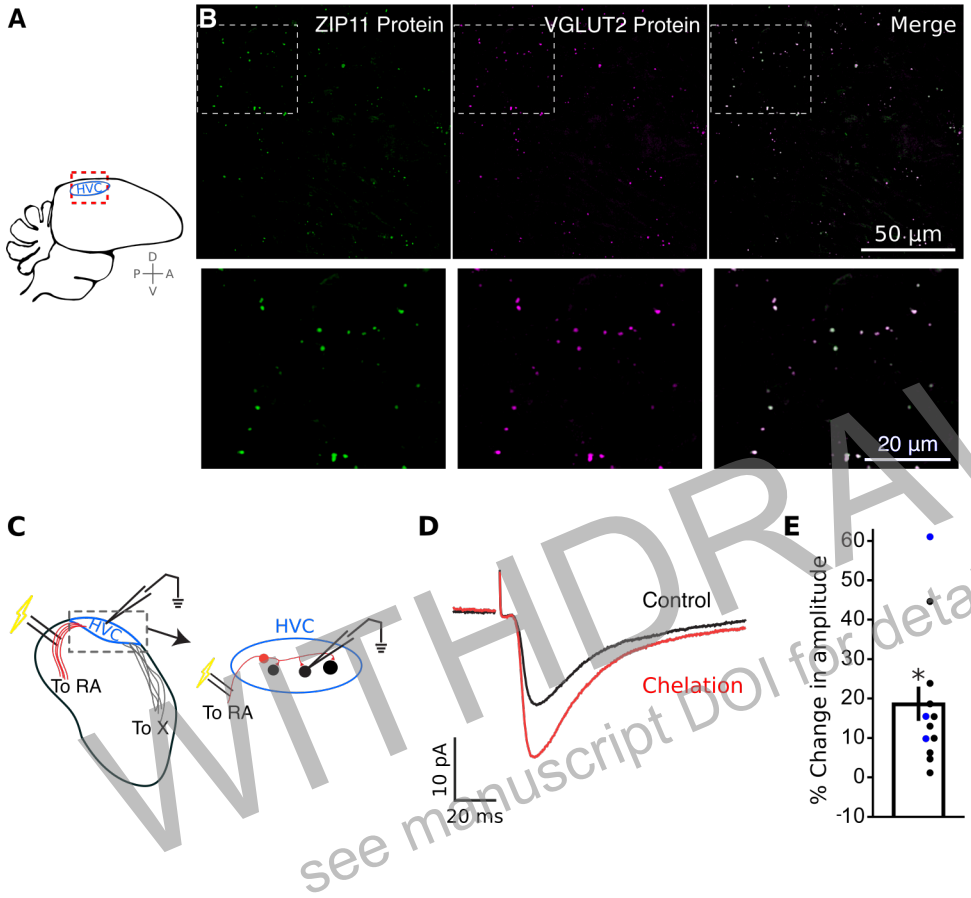

Fig. 3. ZIP11 protein and soluble zinc are in a position to modulate song circuitry.

(A) Sagittal section illustrating the brain area imaged for ZIP11 protein (red). (B) Antibody staining for ZIP11 protein in HVC. Anti-ZIP11 antibody staining is shown in green (left) and anti-VGLUT2 antibody staining (a marker for excitatory synapses) is shown in red (middle). The merged image (right) reveals co-localization between ZIP11 puncta and VGLUT2 puncta, indicating that ZIP11 is present at excitatory synapses. (C-E) Chelation of soluble zinc increased the strength of synaptic currents in HVC. (C) Schematic of *in vitro* slice preparation. HVC-RA neurons were stimulated via the efferent tract to RA, and elicited excitatory post-synaptic currents (EPSCs) were recorded in downstream neurons within HVC. Chelation of zinc increased the amplitude of EPSCs as illustrated for an individual experiment (D) and summarized across experiments (E, blue indicates ZX1, black indicates TPEN, 18 ± 5% increase in peak amplitude, $P < 0.005$, paired *t*-test, n = 12 experiments in 6 birds).

626

627

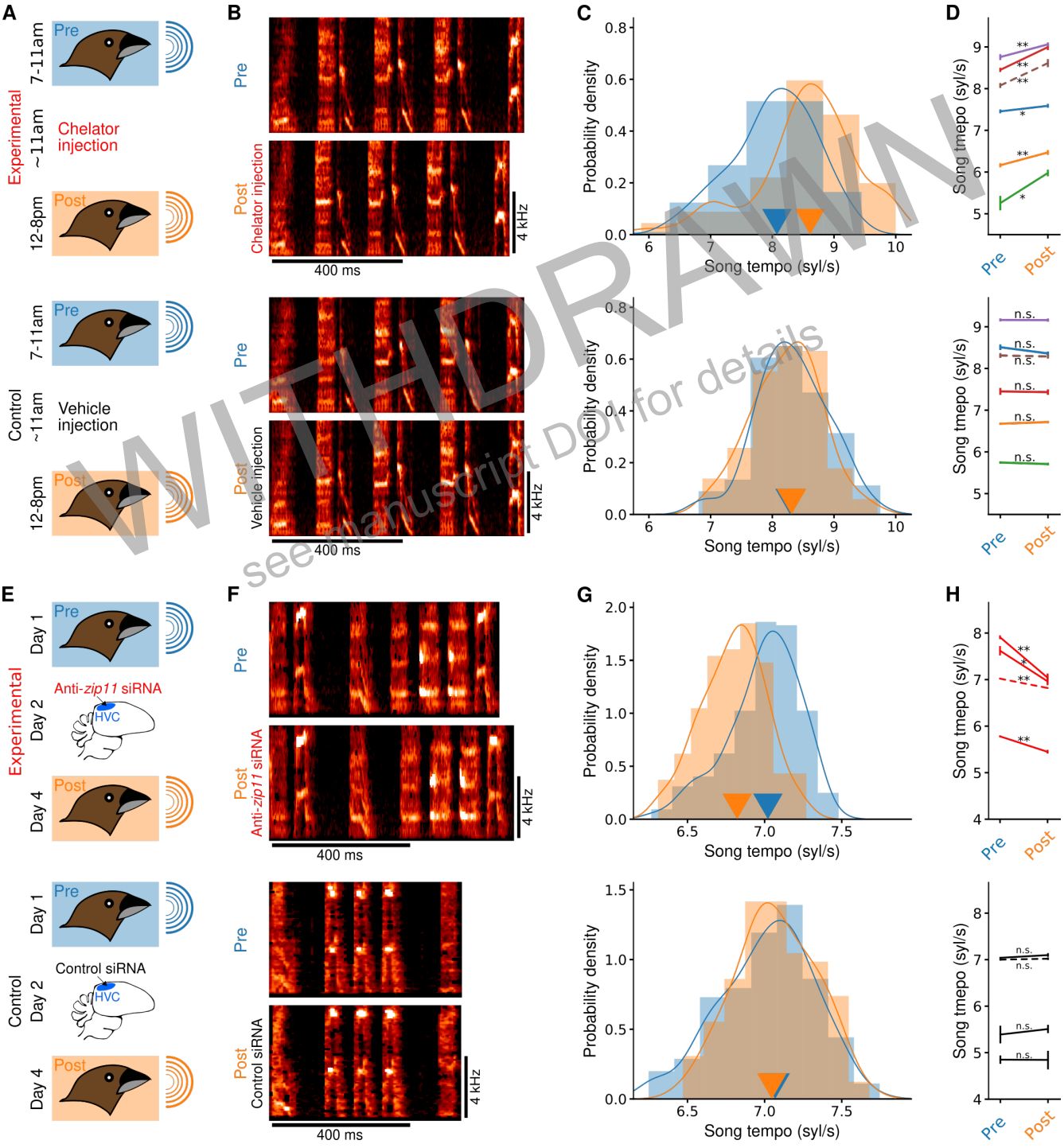

Fig. 4. Manipulations of zinc and *zip11* levels *in vivo* alter song tempo.

(A) Schematic of *in vivo* zinc chelation. In the experimental condition (top), songs were analyzed from blocks 'pre' (7-11am) and 'post' (12-8pm) injection of a solvent carrying the membrane-permeant zinc chelator Clioquinol (CQ). In the control condition (bottom), the same animals were injected with solvent alone. (B) Example songs produced by a bird before and after chelation (top) or control (bottom) manipulation, illustrating that the gross structure of song remained unchanged. (C) The median tempo for this bird increased from 8.08 syl/s 'pre' (blue) to 8.61 syl/s 'post' (orange) zinc chelation. Arrows indicate medians. (D) Median song tempo for each bird pre and post experimental (top) and control (bottom) manipulations. For all birds, the chelator caused a significant increase in song tempo (n = 6; * $P < 0.02$; ** $P < 0.002$, corrected Mood's median test). In contrast, vehicle injection did not affect tempo (n = 6, n.s. denotes $P > 0.1$, Mood's median test). Colors of paired data correspond to individual birds. (E) Schematic of experimental design for ZIP11 knockdown. For the experimental group (top), all songs from day 1 were analyzed as the 'pre' condition. On day 2, HVC was injected bilaterally with anti-*zip11* siRNA. All songs recorded during the first full day of singing following injection (day 4 in all cases) were analyzed as the 'post' condition. For the control group (bottom) treatment was identical except that the siRNA targeted no known Bengalese finch mRNA. (F) Examples of songs produced by two brothers pre and post siRNA injection. For both birds, there was little change to song spectral content. (G) Distribution of song tempos for the same pair of birds before (blue) and after (orange) manipulation. Tempo was slower following injection of anti-*zip11* siRNA (top) but unchanged following injection of control siRNA (bottom). Arrows indicate medians. (H) Median song tempos pre and post injection for 4 pairs of brothers. For each pair, one was injected with anti-*zip11* siRNA (top, $P < 0.002$) while the other was injected with control siRNA (bottom). All animals injected with anti-*zip11* siRNA sang significantly slower following siRNA injection (* $P < 0.02$, ** $P < 0.002$, Mood's median test). Tempo was unchanged by control siRNA (bottom; n.s. denotes $P > 0.1$, Mood's median test). Dashed lines indicate data from the example birds.

Methods

Subjects

Subjects were male and female Bengalese finches (*Lonchura striata domestica*) bred in our colony. They were reared and tutored by their genetic parents to the age of independence. Other than efforts to maintain separation between lineages in order to minimize inbreeding, mating pairs were randomly selected male and female birds. The initial phenotypic analysis (Fig. 1A-1C) used data from 626 male birds and the subsequent linkage analysis used data from 509 birds from families for which we were able to collect DNA markers for male offspring and one or both parents (see below). The Institutional Animal Care and Use Committee at the University of California, San Francisco, approved all protocols.

Audio recording

Vocalizations were digitized at 32 kHz from singly housed birds in sound isolation chambers (Acoustic Systems). Microphones were in a fixed position at the top of the cage housing the bird. Prior to analysis, songs were high pass filtered to capture sound above ~500 Hz. Filters were digitally implemented elliptical infinite impulse response with a passband edge frequency of 0.04 radians. All birds were recorded during early adulthood (90-120 days post-hatch).

Calculation of song tempo

Song tempo was quantified as the average number of syllables produced per second of song, a measure previously shown to be heritable (*29*). Within song, syllables were defined as discrete units of sound separated by silence. Amplitude traces were created by rectifying the filtered song waveform and convolving with a 2 ms square wave. Heuristic thresholds

were set automatically as three times the 10th percentile of values in the amplitude trace. We then identified 'objects' as uninterrupted sounds louder than the threshold and longer than 10ms. We merged any objects separated by silence that was less than 5ms. These final merged objects we defined as 'syllables.' This approach reliably identified syllable onsets and offsets corresponding with those identified by human evaluation. A series of syllables that had no gaps longer than 250ms was considered a song. For each song, tempo was then quantified as the number of syllables present in a given song divided by the duration of that song in ms. For each bird, all summary statistics were derived from at least 60 song renditions.

Chromosome level genome assembly

To generate contiguous DNA sequences that span the length of chromosomes, we combined data from an earlier draft genome assembly of the Bengalese finch genome (*42*) with newly collected data designed to capture local chromosomal architecture. Specifically, we used sequence data from Hi-C (*79*)libraries created by Dovetail Genomics using blood samples we provided. These libraries were sequenced to ~250x coverage using the Illumina HiSeq 4000 platform. This sequence data was then combined with the previous assembly using the Dovetail HiRise assembler. This resulted in a genome assembly with a total length of ~1.06Gb and a total of 2014 scaffolds (RefSeq assembly accession number GCF_005870125.1). The largest 31 scaffolds correspond to Chromosomes 1-15, 17-29 and Z in the Chicken reference genome and additionally to Chromosomes 1a and 4a in the zebra finch reference genome, that were previously created using Sanger sequence data. Together they account for ~97% of the total assembled DNA (National Center for Biotechnology Information BioProject PRJNA369279).

Genetic marker typing

We collected molecular-genetic marker data from each of 509 Bengalese finches used for linkage analysis. These markers were a modified form of Double Digest Restriction Associated DNA (ddRAD) (*80*) markers we call Single End RAD markers (seRAD). From each bird, purified genomic DNA was digested with the non-palindromic restriction enzyme BssS1 (NEB) and the 4 base restriction enzyme Mse1 (NEB) under standard double digest conditions. Digested DNA was purified using the AmpureXP system, ligated (T4 DNA ligase, NEB) to appropriate double stranded linker oligonucleotides (Table S1), then amplified in a 10 cycle PCR reaction using primers that contain an 8bp Illumina i7 compatible barcode and are specific for ligated products that reform the BssS1 and TA sites (Table S1 and S2). Amplified libraries were pooled according to DNA concentration, and size selected (200-500bp) using the BluePippin (Sage Science) system. For each locus digested with the BssS1 enzyme, one of the two ends was sequenced using a custom primer that was specific to one end of the BssS1 cut site and required correct ligation of that site and the appropriate linker (Table S1). For sequencing, 48 samples were multiplexed using the Illumina barcoding system (Table S2). All sequencing was single end 50 or 65 base pairs and performed on the Illumina HiSeq4000 platform. Sequences passing Illumina quality thresholds were then aligned to the Bengalese finch genome (RefSeq GCF_005870125.1) using the MEM algorithm (*81*) from the Burrows-Wheeler Aligner software package (*82*). Across the population of birds, there were ~400,000 distinct genomic loci associated with restriction enzyme cleavage, for each of which 50-65 base pairs were sequenced. Of these, 50,999 loci were identified as potentially informative because they both contained single nucleotide polymorphisms that could serve as markers for transmission of alleles from parents to offspring, and they were sequenced with high coverage in at least 200 individuals. For each individual, the diploid allelic state at each of these informative loci was predicted using the Bayesian framework described in McKenna et al. (*83*). These estimates of diploid allelic state were then used for all subsequent analyses. Across the 509 birds used for genetic mapping, each bird was unambiguously assigned a diploid allelic state at an average of 39,996 ± 221 and a median of 40,827 loci. This corresponds to a marker for allelic state approximately every 25 kilobases across the genome. Each locus was unambiguously assigned a diploid allelic state in an average of 399 ± 0.63 and a median of 473 birds.

Genetic mapping

To establish linkage between regions of the genome and song tempo we used an extension of the Transmission Disequilibrium Test (TDT) appropriate for quantitative phenotypes and able to utilize multiple individuals for each family (*44*). The TDT is a test for genetic linkage and association in outbred populations with known familial structure and uncontrolled breeding (*43*). The TDT statistic at any given locus is calculated only from families with segregation of allelic state at that genomic location and is thus robust to population stratification and missing marker data. In our analysis, we only included genomic locations that, across the entire population, had two (e.g. C/T and C/C) or three (e.g. C/T, C/C, T/T) allelic states comprised of two nucleotides. Where there were three allelic states, the two homozygous states (e.g. C/C and T/T) were used to calculate the TDT as these are the two states where the identities of the parents transmitting the alleles is unambiguous. TDT scores at individual polymorphic locations can be combined to assess the linkage between a larger genomic region and a phenotype (*84*). As each single polymorphic location uses only a subset of individuals from the population, we increased the number of individuals contributing to linkage between tempo and a larger genomic region by combining TDT statistics in sliding windows of 20 markers. The TDT is chi-square distributed and p-values for each 20 marker block were determined from a chi-square distribution with 20 degrees of freedom. This analysis was conducted genome-wide (across 50,999 single loci) on a multi-generational population of 509 (481 males and 28 females) birds where there were 105 unique parental pairs and a median of 4.88 and a maximum of 22 male offspring. Genetic data from all male offspring and (when available) their male and female parents comprised this set.

As both family overlap and genetic linkage between nearby markers may create non-independence among our linkage scores, a genome-wide significance threshold for this analysis was established by permutation test. For each of 10,000 permutations, phenotypes were shuffled relative to genotypes and the entire analysis was re-run. The maximum $-\log_{10} P$ value from each analysis was retained. This set of scores then established a distribution from

760 which significance thresholds were derived. We note that the significance values determined
761 by such permutation testing are conservative relative to those derived by a simple
762 combination of TDT statistic values.

763 **Fluorescent *in situ* hybridization**

764 Fluorescent *in situ* hybridization (FISH) was performed using the hybridization chain
765 reaction system from Molecular Instruments. Birds were euthanized with isoflurane,
766 decapitated, and debrained. Brains were flash-frozen in -70°C dry ice-chilled isopentane for
767 12 seconds within 4 minutes of decapitation, then stored at -80°C. Fresh-frozen brains were
768 cryosectioned at 16 µm onto SuperFrost Plus slides (Fisher), chilled in the cryo-chamber,
769 then melted onto the slide using a warmed metal dowel. Slides were transferred to -80°C for
770 storage. For FISH, slides were transferred from -80°C to slide mailers containing cold 4%
771 formaldehyde and incubated for 15 minutes on ice. After fixation, slides were washed three
772 times for 5 minutes using DEPC-treated PBS + 0.1% TWEEN 20 (PBST), dehydrated in 50%,
773 70%, and two rounds of 100% ethanol for 3-5 minutes each round, then dried in air. Slides
774 were then acetylated for 10 minutes (1.3% triethanolamine, 0.021 N HCl, 0.25% acetic
775 anhydride) and washed in DEPC-PBST for 10 min. Slides were dehydrated again and
776 transferred to a SlideMoat (Boekel Scientific) at 37°C. 100 µL of v3 Hybridization Buffer
777 (Molecular Instruments) was added to each slide, which was then coverslipped and incubated
778 for 10 minutes at 37°C. Meanwhile, 2 nM of each mRNA transcript specific probe was added
779 to 100 µL Hybridization Buffer and denatured at 37°C. Pre-hybridization buffer was removed,
780 100 µL of probe/buffer was added, slides were coverslipped and incubated overnight at 37°C.
781 The next day, coverslips were floated off in Probe Wash Buffer (PWB, 50% formamide, 5x
782 SSC, 9 mM citric acid pH 6.0, 0.1% TWEEN 20, 50 µg/ml heparin), then washed in 75%
783 PWB/25% SSCT (5x SSC, 0.1% TWEEN 20), 50% PWB/50% SSCT, 25% PWB/75% SSCT,
784 100% SSCT for 15 minutes each at 37°C. This was followed by 5 minutes at room
785 temperature in SSCT. Slides were incubated in 200 µL of Amplification Buffer (provided by
786 company) for 30 minutes at room temperature. Alexa fluor-conjugated DNA hairpins were

denatured for 90 seconds at 95°C then allowed to cool for at least 30 minutes in the dark at room temperature. Hairpins were added to 100 ul amplification buffer, applied to slides, and incubated overnight at room temperature. The following day, slides were washed in SSCT containing 1 ng/mL DAPI for 30 minutes at room temperature, then SSCT for 30 minutes at room temperature, followed by a final 5 minutes in SSCT at room temperature. Prolong Glass Antifade Medium (Thermofisher) was added to each slide, which was then coverslipped. Images were acquired using confocal microscopy. The degree of co-localization between objects was evaluated using Mander's co-localization coefficients (*85*).

Immunofluorescent staining

To prepare tissue for staining, birds were deeply anesthetized with isoflurane before being transcardially perfused with 0.9% saline, followed by 3.7% formaldehyde in 0.025 M phosphate buffer. Brains were postfixed for 4–24 h in 3.7% formaldehyde, then cryoprotected in 30% sucrose. Forty micrometer thick sagittal sections were cut on a freezing microtome and stored in phosphate-buffered saline (PBS; 137 mM NaCl, 2.7 mM KCl, 8 mM Na2HPO4, and 2 mM KH2PO4) at 4°C. For immunofluorescence, sections were washed 3 times for 10 min each in PBS at room temperature. Sections were then incubated on a nutator, in clearing reagent, for one hour at room temperature. Clearing agent was either PBS+0.3%triton x-100 (synaptic staining) or PBS+0.1% TWEEN 20 (*SLC39A11* staining alone). Sections were washed 3 times in PBS for 10 min each at room temperature and then transferred to PBS+2% goat serum and incubated for 2-4 hours at room temperature. Sections were transferred to fresh PBS+2% goat serum, and primary antibodies were added at a concentration of 1:500. Sections were incubated in primary antibody overnight at 4°C. The next morning, sections were washed 3 times for 10 min each in PBS at room temperature. Secondary antibodies were added at a concentration of 1:2000, and sections were incubated for 4 hours at room temperature. Following incubation, samples were washed 3 times for 10 min each in PBS at room temperature and transferred to SuperFrost Plus slides (Fisher). Excess fluid was removed, and 40l Vectashield Plus with DAPI (Vectashield) mounting media was added

before coverslips (Fisherbrand, 22mm wide, 0.13-0.17mm thick), which were sealed with clear nail polish. Slides were stored at 4°C. The polyclonal anti-ZIP11 antibody was raised in Rabbits to a fusion protein containing amino acids 93-193 of the Human ZIP11 protein (MyBioSource, MSB1497597). The monoclonal anti-VGLUT2 antibody was raised in Mice immunized to a full length recombinant protein corresponding to rat VGLUT2 (Abcam, ab79157) and has been previously shown to stain VGLUT2 in zebra finches (*86*). The staining patterns of these antibodies were visualized using species appropriate secondary antibodies covalent linked to Alexa fluor 488 or Alexa fluor 633. Images were acquired using confocal microscopy. The degree of co-localization was evaluated using Mander's co-localization coefficients (85).

Electrophysiology

We prepared brain slices from Bengalese finches (60-90 d post-hatch) raised in our breeding colony. Birds were anesthetized with isoflurane and decapitated. Brains were rapidly removed and placed in an ice-cold cutting solution consisting of (in mM): 125 $C_5H_{14}ClNO$, 3 $MgSO_4$, 0.5 $CaCl_2$, 2.5 KCl, 25 $NaHCO_3$, and 35 glucose. Sections (260-300 µm) were cut on a Leica VT1000 microtome. In preparation for electrophysiology, slices were incubated at 36°C in recording ACSF with high magnesium to reduce polysynaptic activity (consisting of (in mM): 125 NaCl, 3 $MgSO_4$, 1 $CaCl_2$, 2.5 KCl, 25 $NaHCO_3$, and 35 Glucose) for 30-60 minutes. Slices were then maintained at room temperature in well-oxygenated (95% O_2-5% CO_2) holding chambers until transfer to the electrophysiological recording chamber. All recordings were made in oxygenated ACSF solution at room temperature (20-25°C). Glass electrodes (3-8 MΩ) were filled with intracellular solution containing (in mM) 120 KGluc, 0.1 EGTA, 40 HEPES, 5 KCl, 0.3 $MgCl_2$. Targeted recordings were made under DIC-IR visualization using an Olympus BX-51 microscope and a camera (FLIR Chameleon). HVC was identified by its visible borders under transillumination. Antidromic stimulation of the HVC neurons projecting to RA was performed with bipolar stimulating electrodes placed in the efferent tract leading to RA (100-150 µm separation, FHC, Bowdoine). Recordings were made with a Multiclamp

700B (Molecular Devices), controlled by custom acquisition software written in Matlab. Pipette capacitance and series resistance were compensated online and series resistance was monitored periodically. Recordings with monotonic changes in input resistance greater than 25% were discarded, as were recordings with monotonic changes in holding current greater than 60pA. Voltage clamp data was acquired at 10 kHz, and filtered at 3kHz. EPSCs were recorded at -70mV in the presence of the GABA-A receptor antagonist, Gabazine (SR-95531, 10-25 µm), in the bath solution. N, N, N', N' -Tetrakis(2-pyridylmethyl)ethylenediamine (TPEN, Sigma) was infused into the bath at 20-100 µm. ZX1 was infused into the bath at 100 µm. The peak amplitude of synaptic events was compared pre and post-chelation. One cell was excluded due to the appearance of an extra EPSC, induced by application of chelator, occurring before the original EPSC preventing an accurate estimate of changes in amplitude.

mRNA transcript preparation and quantification

Fresh coronal sections containing the brain region HVC were cut as described above for electrophysiology, and then transferred to microdissection dishes and kept in ice-cold cutting solution. HVC and the region surrounding HVC were separately microdissected and transferred to a 1.5ml microfuge tube and any remaining cutting solution removed. Immediately afterward, 90ul of TRIzol (ThermoFisher) was added. Samples were then stored at -80°C. When ready for analysis, samples were thawed, and tissue was macerated in the 1.5ml microfuge tube using RNase-free disposable pellet pestles (Fisherbrand). Samples were then incubated at room temperature for 5 min, 20ul chloroform was added, and samples were incubated for a further 2 min. Samples were then centrifuged at 12,000 g and 4°C for 15 min. The aqueous phase was transferred to a new tube, and the organic phase stored at -80°C. Following the addition of 10ug of RNAse free glycogen, the transferred aqueous phase was incubated at room temperature for 1 min. 20ul of isopropanol was added, and the tubes were incubated at room temperature for 10 min. Samples were then centrifuged at 12,000 g and 4°C for 15 min, and the supernatant discarded. The RNA pellet was washed in 100ul

75% Ethanol and centrifuged at 7,500 g and 4°C for 5 min. The supernatant was removed, and the RNA pellet was air-dried and stored at -80°C.

The ProtoScript II (NEB) reverse transcription system was used to create cDNA from RNA samples. For each sample, the entire RNA pellet was solubilized in 6ul RNAse free water, and 2ul of the poly-T reverse transcription primer (d(T)23 VN at 50 µM) was added. RNA/primer mixtures were then denatured at 65°C for 5 min and placed directly on ice. 10µl ProtoScript II reaction mix and 2µl ProtoScript II enzyme mix were added to the RNA/primer mixtures, and the entire reaction was incubated at 42°C for one hour. Samples were incubated at 80°C for 5 minutes to heat inactivate the enzymes, and stored at -80°C.

For each gene, transcript levels were assessed by Quantitative PCR (qPCR). Reactions were performed using the PowerUp SYBR Green Master Mix (ThermoFisher). Each reaction was conducted in triplicate on a 96 well qPCR plate (ThermoFisher). For each replicate reaction, 5µl of master-mix was combined with 1ml template and nuclease-free water to a final volume of 10µl with 400nM final concentration of gene specific primers (Table S3). Each reaction was mixed gently and stored on ice before conducting the qPCR reaction. Reactions were conducted in a QuantStudio 6 Real-Time PCR machine (Applied Biosystems). A standard two step PCR protocol was used. Samples were incubated at 50°C for 2 minutes then heated to 95°C and incubated for 2 minutes. A cycle of two steps was repeated 40 times, in which incubation at 95°C for 15 second was followed by incubation at 60°C for 1 minute. Data from the qPCR reactions were analyzed using the QuantStudio 6 software and cycle threshold (Ct) values were identified for each sample. For each sample, relative Ct values for *SLC39A11* were determined by taking the difference between the *SLC39A11* Ct and the Ct levels of the housekeeping gene PPIA thus controlling for variation in total mRNA input.

Primary neural culture and siRNA screening

All siRNA molecules used for *in vivo* manipulations of gene expression were first screened for efficacy *in vitro*; all sequences were tested for their ability to reduce the targeted gene transcript in cultured Bengalese finch neuronal cells. Prior to cell preparation, tissue culture treated flat bottom 96 well plates (Corning) were incubated in a thin layer of 1mg/ml Laminin (Sigma) solubilized in HBSS with magnesium and calcium (Life Technologies, no phenol red) for 2 hours at 37°C followed by 3 washes in HBSS alone. Chambers were incubated with a thin layer of Poly-L-Ornithine (Life Technologies) at 37°C overnight and washed 3 times with HBSS alone the following day. 1-14 day old birds were euthanized with isofluorane and brains were removed in ice cold HBSS. Following removal of the dura, brain cells were dissociated in pre-warmed papain (Worhtington, 20U/ml in HBSS) at 37°C for 45min. After incubation, tissue was triturated with a 5ml Pasture pipette 15 times then centrifuged at 1200rpm for 5 min. The supernatant was aspirated and the pellet was washed with 7mg/ml Ovomucoid Trypsin inhibitor (Worthington) in HBSS and centrifuged again at 1200rpm for 5 min. Supernatant was aspirated and the pellet was resuspended in 5ml warm, filtered Neurobasal A Complete media (NBAC; Neurobasal A, N2 supplement, B27 supplement, Glutamax, penicillin and streptomycin; Life Technologies). The solution was then triturated 15 times with a fire polished 5ml Pasteur pipette and filtered through a 1000µm cell strainer (Corning). The concentration of cells was measured using a hemocytometer (Fisher Scientific) and cells were diluted to a concentration of $5x10^5$ cells per ml in warm NBAC. 400µl of cell suspension was placed in each well of the 96 well plate and incubated at 37°C for 5 hours at which point the culture media was removed and replaced with 500µl of fresh warm NBAC. Cultures we then incubated at 37°C and 5% CO_2. 50% of media was exchanged every 3-4 days.

Once neural processes formed (after ~1 week) the cell cultures were used to test siRNA molecules. For each siRNA tested, knockdown experiments were conducted in duplicate using the RNAiMAX (Life Technologies) transformation reagent. For each siRNA 25µl of Opti-MEM Medium (Life Technologies) was mixed with 1.5µl of RNAiMAX reagent. Separately, 25µl of Opti-MEM Medium was mixed with 5pmol paired siRNA molecules (Dharmacon). These two mixtures were then combined and incubated at room temperature

for 5min. Following incubation, 10µl of the RNAiMAX/siRNA mixture was added to each of two wells of neural cell culture. Cultures were then incubated at 37°C and 5% CO_2 for 2 days. After incubation, RNA from each well was purified, converted to cDNA, and quantified using the protocol described in mRNA transcript preparation and quantification (above). The mRNA expression level of the 'target' gene was compared between cells exposed to experimental siRNA molecules and cells exposed to a control siRNA molecule. The siRNA resulting in maximal knockdown of *SLC39A11* transcript (Table S4 and Fig. S4) was then used for all *in vivo* experiments.

siRNA injections

Prior to injection, siRNAs were complexed with the transfection reagent BrainFectIN (Oz Biosciences). siRNA molecules were added to BrainFectIN at a ratio of 1 µg siRNA:1.5 µg BrainFectIN and incubated at room temperature for 20 min and then used within 20min. Concurrently, birds were deprived of food and water for 1 hour, and then anesthetized with an intramuscular injection of 30–40 µl of equithesin (0.85 g of chloral hydrate, 0.21g of pentobarbital, 0.42g of $MgSO_4$, 2.2 ml of 100% ethanol, and 8.6 ml of propylene glycol to a total volume of 20ml with water). Following craniotomy and removal of the dura, siRNA complexes were injected into HVC bilaterally. The stereotactic coordinates used were 2.0ml medial/lateral, 0 dorsal/ventral relative to the y-sinus, with the head oriented with a beak angle of 50 degrees. siRNA complexes were introduced at multiple points between 700-250 µm below the surface of the brain using a Nanoject-2 (Drummond Scientific), culminating in a total injection volume of 10 µl per hemisphere. In each hemisphere, after the final injection, the pipette was left in place for ~10 minutes before full retraction. Baseline, 'pre' manipulation song tempo data was collected for a full day prior to injection, and 'post' manipulation data was analyzed from the first full day of singing (the second day post-surgery in all cases). All siRNAs were synthesized by Dharmacon. Control and experimental siRNA sequences are presented in Supplemental Table 4.

947 **Clioquinol injections**

948 Clioquinol (CQ) was solubilized in DMSO at a concentration of 40mg/ml. For all birds
949 and all experiments, 6 µl of either DMSO or DMSO+CQ was injected intramuscularly at 11
950 am. The tempo of songs produced before 11am were then compared to the tempo of songs
951 produced after 12pm.

Supplementary Figures

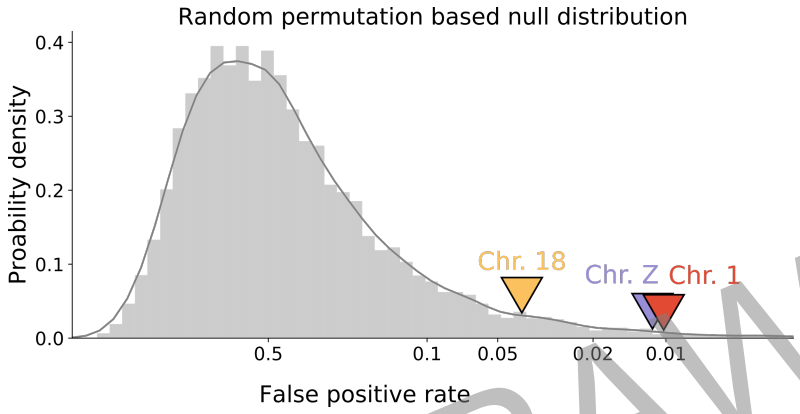

Fig. S1. Permutation based genome-wide null probability distribution for association between song tempo and allelic state.

Null probability distribution resulting from 10,000 permutations of the complete linkage analysis as shown in Figure 1D. Before each permutation, the phenotype and bird identity were randomly shuffled; thus, each analysis retained the genetic architecture of the overall population but dissociated this architecture from song tempo. The distribution comprises the TDT statistic for the single most significant sliding window (of 20 makers) from each permutation. Critical values for genome-wide significance were calculated as the 100*(1-α) percentile of this distribution where α is the false positive rate. Colored arrows indicate the most significant sliding window for each of three regions (see Figure 1) significantly linked to song tempo.

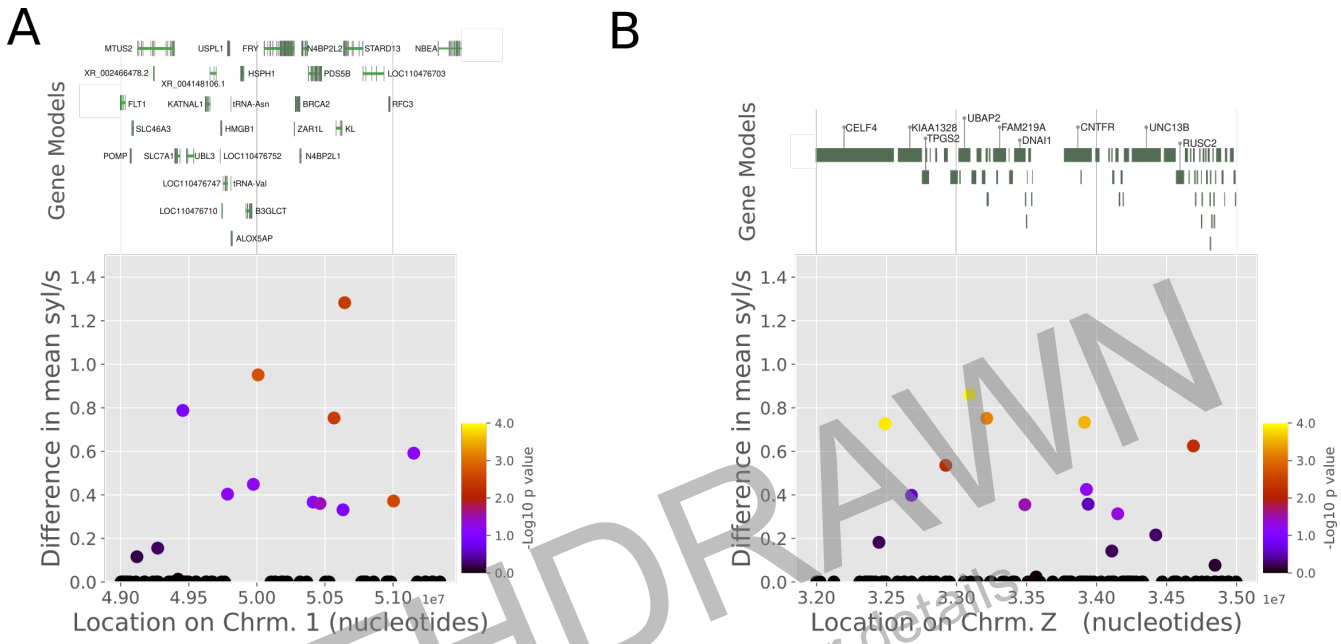

Fig. S2. Effect size associated with individual markers within genomic regions on Chromosomes 1 and Z.

Difference in mean phenotype associated with allelic state at polymorphisms within regions on Chromosome 1 (A) and Chromosome Z (B) that were significantly linked to song tempo. P values for linkage at each locus are indicated by the color of the corresponding point and the heat maps at right. Gene models within each region as determined by genome annotation (National Center For Biotechnolgy Information BioProject PRJNA369279) are indicated at top. Detail for gene models are adjusted due to differences in gene number and density. Coding (dark green) and intronic (light green) regions are indicated in A while the length of a gene model (both coding and non-coding) are indicated by dark green in B.

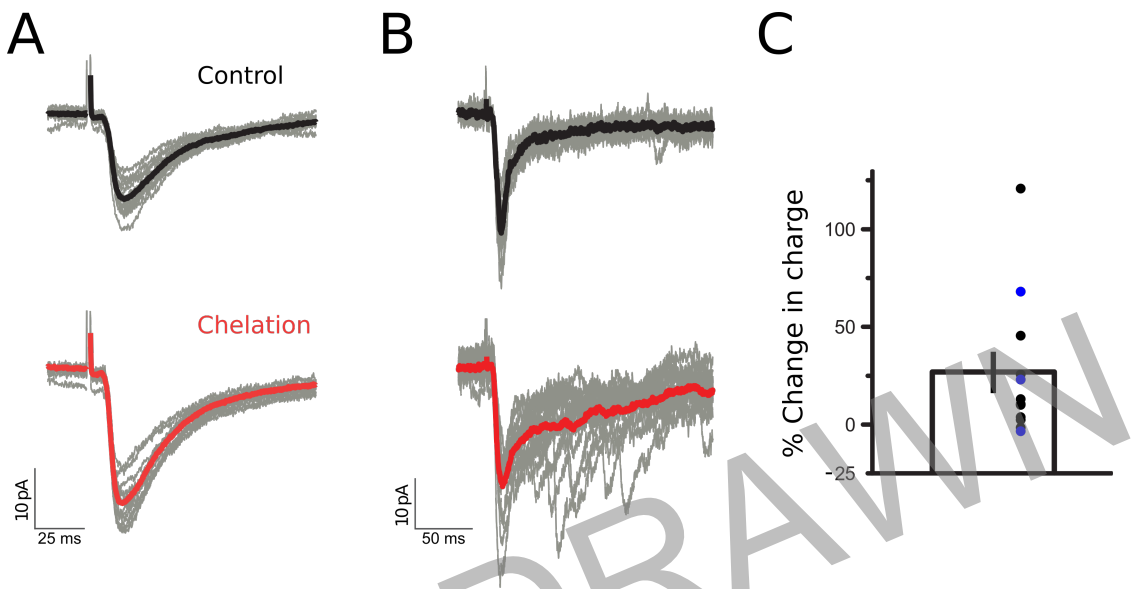

Fig. S3. Zinc chelation increases synaptic currents in HVC.

(A-B) Chelation of zinc increased the amplitude of synaptic events as illustrated for an individual experiment (A) and, in some cases, increased the number of synaptic evens as shown in a different experiment (B). (C) Summary of increased synaptic charge transfer across experiments (blue indicates ZX1, black indicates TPEN, 26.5 ± 10% increase in total charge transfer, $P < 0.01$, paired *t*-test, n = 12 experiments in 6 birds).

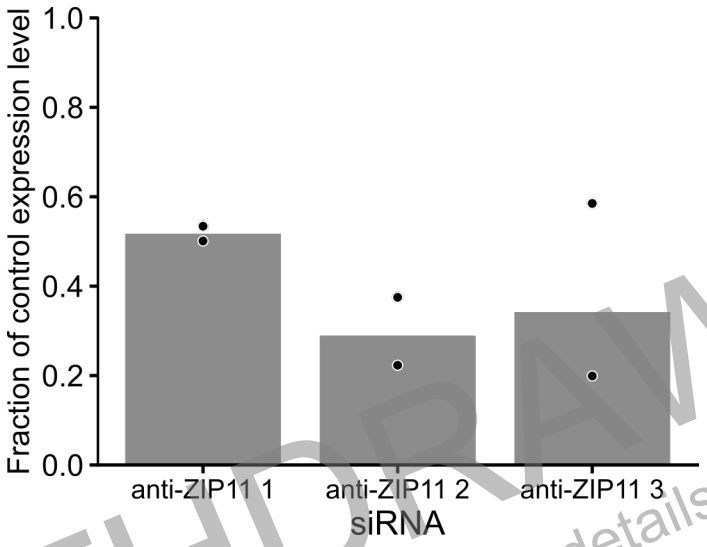

Fig. S4. Fraction of *zip11* expression following siRNA mediated knockdown in neural culture.

Fraction of control expression level of *zip11* following knockdown with one of 3 siRNAs. Expression following knockdown is normalized to levels from neural culture exposed to a control siRNA (supplemental table 4) designed to target no known Bengalese finch transcript.